Microbial Volatile Organic Compound (VOC)-Driven Dissolution and Surface Modification of Phosphorus-Containing Soil Minerals for Plant Nutrition: An Indirect Route for VOC-Based Plant-Microbe Communications

Bacterial VOC-driven surface engineering of phosphorus-containing soil minerals and its impact on plant growth: an indirect route for VOC-based plant-microbe communications

Anahita Barghi[1], anahitabp@postech.ac.kr
Lorenzo Degli Esposti[2], lorenzo.degliesposti@istec.cnr.it
Michele Iafisco[2], michele.iafisco@istec.cnr.it
Alessio Adamiano[2], alessio.adamiano@istec.cnr.it
Guillermo Escolano Casado[3], guillermo.escolanocasado@unito.it
Pavlo Ivanchenko[3,4], pavlo.ivanchenko@vub.be
Lorenzo Mino[3], lorenzo.mino@unito.it
Ho Young Yoon[5], dbsghdud0601@naver.com
Eun-Nam Joe[5], 0109785@naver.com
Jong-Rok Jeon[5,*], jrjeon@gnu.ac.kr
Yoon-Seok Chang[1,*], chang.yoonseok@postech.ac.kr

Affiliations

[1]Division of Environmental Science and Engineering, Pohang University of Science and Technology (POSTECH), 77 Cheongam-ro, Pohang, 37673, Republic of Korea
[2]Institute of Science and Technology for Ceramics (ISTEC), National Research Council (CNR), Via Granarolo 64, 48018 Faenza (RA), Italy
[3]Department of Chemistry and NIS Centre, University of Torino, via Giuria 7, 10125 Torino, Italy
[4]Vrije Universiteit Brussel (VUB), ETEC department, MOBI research group, Pleinlaan 2, 1050 Brussels, Belgium
[5]Division of Applied Life Science (BK21Ps), Department of Agricultural Chemistry and Food Science & Technology and IALS, Gyeongsang National University, Jinju 52828, Republic of Korea

*Correspondance: J.-R. Jeon and Y.-S. Chang

Abstract

Microbial volatile organic compounds (MVOCs) are believed to act as remote messengers in the interaction with plants, resulting in physiological changes in terms of plant growth and stress resistance. However, it remains unclear whether plants directly detect MVOCs using dedicated sensing machinery or whether other factors mediate this communication process. We investigated the ability of MVOCs secreted by *Bacillus megaterium* (a well-known MVOC producer) to modify the solid surface of hydroxyapatites, a widespread group of soil minerals. FT-IR spectral results indicated the spontaneous localization of MVOCs on the apatite surface based on variation in the COO^- band with incubation time. The MVOCs facilitated the release of soluble phosphate from the minerals in a time-dependent

manner. The formation of calcium oxalate was revealed through SEM-EDS and XRD analyses, suggesting that the MVOC oxalic acid can block the recrystallization of phosphate into calcium phosphates. Gel- and soil-based plant cultivation tests employing *Arabidopsis thaliana* and solid calcium phosphates (*i.e.*, nano- and micro-sized hydroxyapatites and calcium phosphate dibasic) revealed that these MVOC mechanisms facilitated plant growth by ensuring the prolonged supply of plant-available phosphorus. The relationship between the enhancement of growth and the particle size of the calcium phosphates also substantiates the sorption of MVOCs onto soil minerals related to plant growth. Given that most previous studies have assumed that MVOCs are a molecular lexicon directly detected by plants, our approach provides a new mechanistic view of the presence of abiotic mediators in the interaction between plants and microbes via MVOCs.

Keywords: microbial volatile organic compounds, calcium phosphate, surface engineering, plant nutrition, plant-microbe interaction

Introduction

Microbial volatile organic compounds (MVOCs) are low-molecular-weight microbial metabolites derived from various synthetic pathways for aliphatic amino acids, fatty acids, terpenoids, pyrazines, and aromatic compounds (Schulz et al., 2020). In nature, MVOCs can move far from their site of production via the air, water, and pores in the soil, thus allowing microbes to interact with other biological species at a distance (Kanchiswamy et al., 2015). MVOCs appear to be particularly important in plant–microbe communications because, with the exception of epiphytes, the limited mobility and small size of microbes restrict physical contact with plants. In fact, scientific evidence supporting MVOC-driven plant–microbe interactions is abundant, with many microbial genera including *Arthrobacter*, *Pseudomonas*, *Bacillus*, *Trichoderma*, *Paraburkholderia*, and *Paenibacillus* shown to be capable of producing organic volatiles that modulate plant growth and stress resistance (Fincheira et al., 2018; Lee et al., 2012; Weisskopf et al., 2021). For example, several kinds of organics (*e.g.*, 2,3-butanediol, indole, dimethyl disulfide, and pentadecanol) in MVOCs are found to facilitate root, leaf, and shoot growth and chlorophyll production, which is accompanied by variation in a wide range of genetic expressions associated with photosynthesis, cell wall synthesis, and auxin hormone responsiveness (Fincheira et al., 2018). The resistance of plants to biotic (*e.g.*, pathogens) and abiotic (*e.g.*, drought and salt) stresses is promoted by MVOCs via the induction of systemic resistance, the synthesis of compatible solutes, and changes in sodium transporter expression (Liu et al., 2015; Weisskopf et al., 2021).

Harnessing these effects of MVOCs on plants has been regarded as a promising strategy for sustainable agricultural practices, but detailed mechanistic explanations for how plants detect MVOCs still remain to be elucidated. It has

been hypothesized that plants inherently possess dedicated sensing machinery but, to the best of our knowledge, no molecular evidence has been reported to date. Moreover, MVOCs are structurally versatile, and a variety of MVOCs are produced simultaneously, meaning that it would be difficult for plants to directly detect them. Alternatively, other possible mechanisms could be non-specific interactions between organic moieties frequently found in MVOCs and plant components or that other factors controlled by MVOCs mediate plant–microbe interactions. It has been demonstrated that cellular membranes can be damaged by the penetration ability and non-specific binding of MVOCs to membrane components (Trombetta et al., 2015), indicating that initial non-specific stress- or toxicity-related responses can translate into MVOC-induced changes in plant physiology. Moreover, Jones et al. (2019) reported that trimethylamine (TMA), an MVOC produced by *Streptomyces*, alters iron availability by changing the environmental pH. Plant nutrition and associated plant physiology can be subsequently affected by changes such as this, thus other soil-related factors could be investigated as potential mediators to account for plant–microbe communications.

MVOCs containing oxygen-based functional groups, which derive from the primary, fatty acid, and aromatic metabolism of microbes, are easily detected in the plant-microbe interactions (Weisskopf et al., 2021). Interestingly, these MVOCs are structural parallels to some organics associated with the surface engineering of metallic minerals found in soil environments. For example, stearic acid-modified apatite surfaces lead to dispersion in non-polar matrices (Li et al., 2008), and the spontaneous localization of citric acid on apatite surfaces is feasible when modulating the kinetics of apatite dissolution (Samavini et al., 2018; Schutze et al., 2020). Oxalic acid is also capable of modifying mineral surfaces, including silicate, gangue, and ilmenite, which consequently affects their floatation behavior (Nuri et al., 2019). It has been reported that gluconic acid has a role in phosphate solubilization (Lin et al., 2006; Rodriguez et al., 2004; Stella and Halimi., 2015). These non-specific actions associated with several minerals appear to exploit the ability of oxygen-based functional groups within MVOCs to facilitate coordination, hydrogen bonding, and dipole–dipole interactions. It is also important to note that these modifications coincide with changes in plant growth and physiology. Acidic oxygen-based functional groups can solubilize the surface of minerals, leading to the release of diffusible ions. In particular, phosphate, an important plant nutrient, is efficiently released in this manner. This surface engineering-based action can also be prolonged in a time-dependent manner (Samavini et al., 2018; Schutze et al., 2020; Wang et al., 2016), suggesting that soil quality evolves in terms of plant nutrition. Indeed, it has been demonstrated that plant nutrition directly affects plant growth, development, and stress resistance (Feller et al., 2018). Expression of diverse sets of genes and proteins is also modulated with plant nutrition (Brumbarova et al., 2019).

Given the structural similarities between known MVOCs and organic compounds capable of mineral surface engineering, it is highly likely that a significant proportion of MVOCs play a crucial role in modifying mineral surfaces in soils. The mobility of MVOCs means that they can diffuse into the plant rhizosphere, subsequently modifying the surface of minerals required for plant nutrition. Because the effects of plant nutrition (*e.g.*, plant growth and stress resistance) are similar to the observations reported in previous studies that posit the direct sensing of MVOCs by plants

(Sharifi., 2018; Weisskopf et al., 2021), it is important to investigate the possibility that MVOCs are also involved in plant–microbe communications via the modification of minerals employed in plant nutrition. This study thus aimed to confirm whether the surface characteristics of solid ceramic particles are modified by MVOCs. Calcium phosphate and *Bacillus megaterium* were selected as the model ceramic and microorganism, respectively. After measuring phosphate release kinetics of calcium phosphate before and after MVOC treatment, Fourier-transform infrared spectroscopy (FT-IR) and X-ray diffraction (XRD) were employed to characterize the effects of MVOCs on the mineral surface. Finally, the growth of *Arabidopsis thaliana* was assessed to evaluate the potential of MVOC-driven mineral surface modification as an abiotic mediator facilitating plant–microbe communications.

Materials and methods

Chemicals and materials

Bacillus megaterium GNU-01 was isolated from commercial humic acids and deposited at the Korean Collection for Type Cultures (No. 13087BP). Wild-type *A. thaliana* (Col-0 background) was kindly donated by Dr. Joon-Yung Cha (Gyeongsang National University, Jinju, Republic of Korea). Murashige and Skoog (MS) medium, calcium phosphate dibasic (purum p.a., ≥85%), micrometric hydroxyapatite (HA; $Ca_{10}(PO_4)_6$, reagent grade), vanadate-molybdate (p.a. for phosphate determination), calcium hydroxide ($Ca(OH)_2$, ACS reagent, ≥95%), phosphoric acid (H_3PO_4, ACS regent, ≥85%, potassium bromide (KBr, FT-IR grade, ≥99 trace metal basis), hydrochloric acid (HCl, extra pure grade), sodium bicarbonate ($NaHCO_3$, ACS reagent, ≥99.7%), nutrient broth, and sodium hydroxide (NaOH, reagent grade, ≥99.7%), were purchased from Sigma-Aldrich. Plant agar and sucrose were purchased from Duchefa-Biochemie, and bed soil and potassium chloride (KCl) were purchased from Nongwoo Bio (Suwon, Republic of Korea) and Namhae Chemical (Yeosu, Republic of Korea), respectively. Unless otherwise noted, ultra-pure water (Milli-Q, Millipore) was used in the experiments and all reagents were used as received without any extra purification.

Plant and bacteria cultivation

Bacillus megaterium was cultured in a 250 mL Erlenmeyer flask containing 100 mL of nutrient broth. The flask was kept in a shaking incubator (160 rpm) at 32 °C for 24 h before use. Plant cultures were created using MS medium containing 0.9% (*w*/*v*) agar and 2% (*w*/*v*) sucrose with the pH adjusted to 5.8 unless otherwise mentioned. The surface of the seeds was sterilized with 70% ethanol for 30 s and then 20% Clorox for 5 min followed by repeated washing with distilled water. After sowing, the plates were vernalized for 2 days at 4 °C in the absence of light and transferred to a conventional plant chamber (23 °C and 16/8 h light/dark cycle). In addition, MS medium that had been modified to remove phosphorus (P) was mechanically mixed with HA nanoparticles (HANPs) to ensure that the HANPs were the only source of P for plant nutrition.

***Bacillus megaterium* VOCs profiling**

Bacillus megaterium was cultured in 20 ml glass vials containing MS agar. The vials were tightly sealed with a steel crimp cap fitted with a Teflon/silicon septum to minimize VOC leakage. Solid-phase microextraction (SPME) was then conducted using flexdivnylbenzene/carboxen/polydimethylsiloxane (50/30 lm) fibers (Supelco). The microbial colony-bearing agar was warmed to 80 °C and the SPME fibers were injected into the headspace for 20 min. The VOCs on the SPME fibers were then desorbed and profiled using gas chromatography–mass spectrometry (GC-MS, QP2020NX, Shimadzu) equipped with a DB5-WAX column (30 m, 0.25 mm id., 0.25 um film thickness, Agilent). The oven temperature started at 40 ºC for 3 min and was increased to 80 °C at a rate of 7 °C/min and then to 240 °C at a rate of 25 °C/min, where it was held for 5 min. An electron impact method was used to obtain the mass-to-charge ratio (*m/z*) from 40 to 500, and the mass fragment patterns for each significant peak were compared with those in the NIST database.

Hydroxyapatite nanoparticle synthesis

HANPs were synthesized using a modified version of the neutralization method described by Adamiano et al. (2017). Briefly, solution A was obtained by adding 10 g of $Ca(OH)_2$ to 100 mL of distilled water followed by stirring at 400 rpm for 30 min to produce a homogenous solution. Solution B comprising 8.87 g of H_3PO_4 dissolved in 30 mL of distilled water was added slowly to solution A under constant stirring at 400 rpm for 180 min followed by incubation overnight at room temperature. The Ca:P ratio was set at 1.67 mole/L for synthesis. The nanoparticle powder was washed thoroughly with distilled water and air-dried at 40 ºC.

Phosphate release analysis

Biplates containing two physically separated spaces were used to assess the effects of MVOCs on the phosphate release of HANPs. One space contained HANPs (0.7 g) dispersed in 15 mL of distilled water, while the other space held MS agar that had been inoculated with 15 µL of *B. megaterium* (approximately 1×10^9 CFU) in a dropwise manner. The pH and phosphate concentration were examined weekly for up to 8 weeks and compared with those for a HANP dispersion without bacteria. The release of phosphate from the HANPs was measured using a vanadate/molybdate method. Briefly, the supernatant of the HANP suspension was harvested weekly using centrifugation (13,000 rpm and 10 min), with 1 mL aliquots filtered using a syringe filter (0.2 µm) and then mixed with 250 µL of vanadate–molybdate reagent. After 10 min at room temperature, the absorption was recorded at 470 nm with a conventional UV-visible spectrophotometer. The separated HANP pellets were re-suspended in fresh distilled water.

Effect of *Bacillus megaterium* VOCs on HANP mineralogy

For instrument-based analysis, the HANP solutions were treated with KCl to raise their ionic strength to 0.01 mole/L. The particles were then harvested using centrifugation (3,000 rpm and 20 min) followed by drying at room temperature.

Fourier-transform infrared spectroscopy analysis

For all the FT-IR spectroscopic measurements, HANP powder, after exposure to the microbes for 7, 14, or 28 days, was pressed into self-supporting pellets and placed in quartz IR cells designed for spectroscopic measurements at room temperature (*i.e.*, cells equipped with KBr windows). The cells were connected to a conventional vacuum line (residual pressure = 1×10^{-3} mbar) to perform all *in situ* treatments and adsorption–desorption experiments. The spectra were collected at a resolution of 4 cm^{-1} with a Bruker Invenio R spectrometer equipped with a DTGS detector. The number of scans was adjusted to 64 s^{-1} to attain a suitable signal-to-noise ratio. The data were normalized to the optical density (*i.e.*, the weight of the pellet in mg/the area of the pellet in cm^2) to account for differences in the thickness of the pellets. The HANPs were exposed to water (H_2O) or heavy water (D_2O) vapor pressure at the beam temperature (ca. 50 °C) and then outgassed for 3 h. To achieve the complete exchange of H_2O with D_2O, the sample underwent a series of heavy water admission/outgassing steps until the invariance of the spectra. For the adsorption of oxalic acid, the pellet was placed at the top of a closed chamber that had 200 mg of oxalic acid crystals at the bottom. The chamber was placed in an oven at 80 °C for 4 h, saturating the chamber with oxalic acid vapor and allowing the adsorption of oxalic acid on the HANP surface.

X-ray diffraction analysis

Each sample was analyzed using XRD with a D8 Advance diffractometer (Bruker, Karlsruhe, Germany) equipped with a Lynx-eye position-sensitive detector using Cu Kα radiation (λ = 1.54178 Å) generated at 40 kV and 40 mA. The XRD profiles of the samples were acquired using a step size (2θ) of 0.02° and a counting time of 0.5 s in a 2θ range of 10−60°. Phase identification was conducted with Highscore software (PANalytical) and powder diffraction files (ICDD PDF4+ 2013).

Equation (1) was used to calculate the crystallinity of each sample:

$$\text{Crystallinity [\%]} = 100 \cdot C/(A+C) \quad (1)$$

where *C* is the sum of the peak areas and *A* is the area between the peaks and the background in the diffraction patterns (Adamiano et al, 2013).

Scanning electron microscopy

The morphology of the samples was investigated using scanning electron microscopy (SEM) with a field-emission microscope (FE-SEM, ΣIGMA, ZEISS NTS Gmbh, Oberkochen, Germany) coupled to an energy-dispersive X-ray

spectrometer (EDS; INCA Energy 300, Oxford Instruments, Abingdon-on-Thames, UK). A small quantity of the material was placed on carbon tape supported by an aluminum SEM stub for sputter-coating (Polaron E5100, Polaron Equipment, Watford, Hertfordshire, UK) with a 10 nm layer of gold for electrical conductance. A 3 kV accelerating voltage was used for sample observations in secondary electron imaging mode. Four random regions of the stub were imaged at magnifications of 5000×, 15,000×, 25,000×, and 50,000× for each sample. The elemental composition of the samples was analyzed using SEM-EDS with non-sputter-coated HANPs. An acceleration voltage of 10 kV was used to collect spectra from a minimum of four randomly selected regions of the samples at magnifications of 10,000×.

Bioavailability analysis

To assess whether the MVOC-mediated solubilization of HANPs is involved in plant nutrition, modified MS medium whose phosphate ions had been replaced with HANP particles (*i.e.*, 0, 2, 6, and 18 mg of HANPs in 15 mL of MS medium) was used to cultivate *A. thaliana*. Fourteen-day old *A. thaliana* seedlings were transferred to one half of a biplate containing the modified MS medium, with the other half containing normal MS agar inoculated with *B. megaterium* (approximately 1×10^9 CFU) in a dropwise manner. The plates were incubated in a plant growth chamber (23 °C with a 16/8 h light/dark cycle). The fresh and dry weights (70 °C for 24 h) of the plants were compared with those of controls cultivated without the microbes and/or the HANPs. To measure pH and phosphate concentrations, agar slices from each plate were transferred to conical tubes after removing the plants and heated until the agar had completely melted. The pH was measured using a regular pH electrode, and phosphate was measured using the vanadate–molybdate method described above.

Soil systems were also created by mixing air-dried soil particles (50 g) with calcium phosphate powder (*i.e.*, 3 or 6 mg of HANPs, calcium phosphate dibasic, or micrometric HA). A Petri dish (6 mm) containing normal MS agar inoculated with *B. megaterium* (approximately 1×10^9 CFU) was placed at the bottom of the soil pot, thus allowing the microbes to emit MVOCs toward the soil. Sterilized *A. thaliana* seeds were sowed and then incubated in a plant chamber (23 °C with a 16/8 h light/dark cycle) for two months. Total P was obtained from 0.25 g of the soil from each pot, which was heated to 550 °C for 1 h followed by mixing the resulting dried soil with 25 mL of 1 M HCl. The mixture was incubated for 16 h at 60 °C. P content was estimated using inductively coupled plasma-optical emission spectrometry (ICP-OES, Thermo Scientific-United States) with 0.2 μm-filtered solutions. Available P was measured by adding 40 mL of 0.5 M $NaHCO_3$ to 0.5 g of soil. The pH was then adjusted to 8.5 with 1 N NaOH followed by gentle shaking for 16 h at room temperature. After centrifugation (3000 rpm and 5 min), the P in the supernatant was quantified using ICP-OES (Wuenscher et al., 2015; Zhao et al., 2018).

Results and Discussion

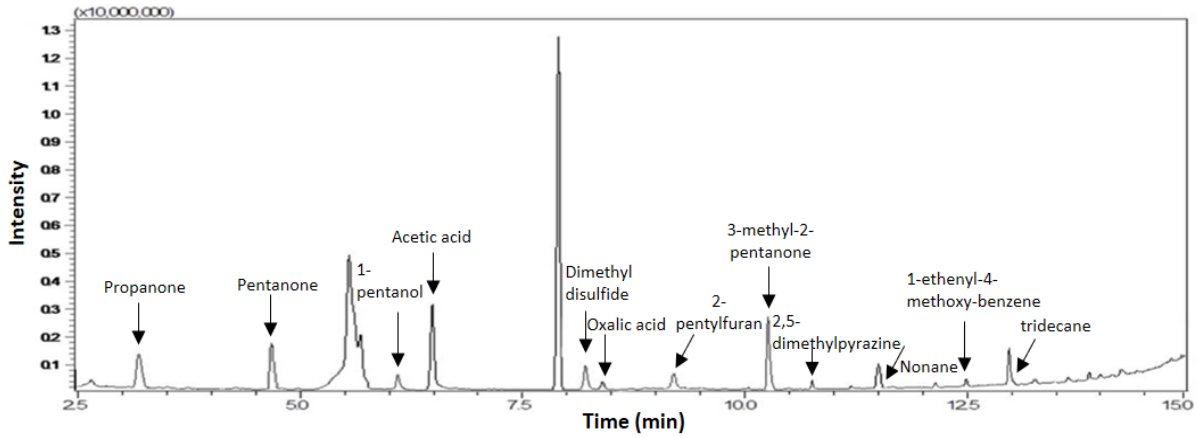

Figure 1. GC-MS profiling of VOCs emitted from *Bacillus megaterium*

MVOCs from *B. megaterium* were identified to evaluate whether the microbe has the potential to stimulate plant growth with airborne molecules. As shown in **Fig. 1 and Table S1**, six groups of compounds with 12 distinct organic structures were detected, including three ketones (propanone, 2-pentanone, and 3-methyl-2-pentanone), two organic acids (acetic acid and oxalic acid), one alcohol (1-pentanol), one sulfur-containing compound (dimethyl disulfide), three aromatics (2-pentylfuran, 2,5-dimethylpyrazine, and 1-ethyl-4-methoxy-benzene), and two alkanes (nonane and tridecane). Some of these, including dimethyl disulfide, pentanone, and pentanol, have been previously reported to promote plant growth and systemic resistance through airborne pathways (Choi et al., 2014; Kanchiswamy et al., 2015). It is also noticeable that small oxygen-containing organic compounds such as oxalic acid, acetic acid, and pentanol are produced as organic volatiles, as described previously for other microbes (Schulz et al., 2020; Weisskopf et al., 2021).

Previous studies have shown that the bioavailability of P from rock phosphate and P-containing ceramics is higher in the presence of oxygen-containing organic compounds (Wang et al., 2016; Jamal et al., 2018). The relatively low pK_a of alcohols and carboxylic acid leads to a more acidic soil environment, thus facilitating the dissolution of P-containing solids. Another effect of small organic acids such as oxalic acid and citric acid is their spontaneous adsorption onto the surface of apatites (Samavini et al., 2018). Due to this surface engineering, the time-dependent release of phosphate ions has been observed, accompanied by enhanced plant growth (Samavini et al., 2018; Yoon et al., 2020; Yoon et al., 2021). This indicates that the MVOCs detected in the present study could be involved in the mobilization of inorganic nutrients in soil environments. To directly prove this, HANPs were tested because calcium phosphates are widespread in soils and act as a source of P for plant nutrition (Chang and Jackson, 1957).

As shown in **Fig. 2**, the pH of aqueous solutions containing HANPs treated with MVOCs was significantly lower than that of the controls. Based on the identification of MVOCs containing alcohol and carboxylic acid (**Fig. 1**), this phenomenon could be attributable to MVOC-induced acidity. The release of phosphate from the HANPs was also improved by MVOC treatment, while the release without microbial treatment was very low (**Fig. 2**). The dependence of HANP dissolution on pH has been well-characterized (Wang et al., 2016), meaning that the enhanced release likely resulted from more rapid particle dissolution.

To investigate MVOC binding on the surface of HANPs, FT-IR was used to identify the carboxylic groups before and after MVOC treatment. **Fig. 3** shows that the surface of the particles contained a significant quantity of carboxylic acids. FT-IR spectra were collected after outgassing the samples as such (**Fig. 3A**) and after the exchange with heavy water (**Fig. 3B**). In **Fig. 3A**, a broad band from ca. 3700 to ca. 2750 cm^{-1} was observed for all spectra, due to the ν(OH) stretching modes of hydrogen-bonded water molecules adsorbed onto the surface of the HANPs (Mino et al., 2020). The narrow peak at 3569 cm^{-1} was ascribed to the vibrations of columnar OH in the HA in the 4e position within the hexagonal lattice (Sakhno et al., 2015).

In the 2200–1900 cm^{-1} range, signals from the combination and overtones of the vibration modes of bulk phosphate groups were observed (Diallo-Garcia et al., 2014). A band associated with the δ(HOH) bending mode at 1645 cm^{-1} was also clearly observed in the control samples, and this signal overlapped with the antisymmetric stretching mode $\nu_{asym}(COO^-)$ from carboxylic species adsorbed onto the surface of the HANPs in the samples treated with MVOCs (Achelhi et al., 2010; Mino et al., 2016). This vibration ($\nu_{asym}(COO^-)$) was coupled with the symmetric stretching mode $\nu_{sym}(COO^-)$ present as a narrow band centered at 1322 cm^{-1} for 7B and 14B and as a doublet at 1322 and 1328 cm^{-1} for 28B. Additionally, an intense band due to carbonate species was present in the 1540–1350 cm^{-1} range, originating from the CO_2 dissolved introduced during the preparation of the materials (Fleet et al., 2009).

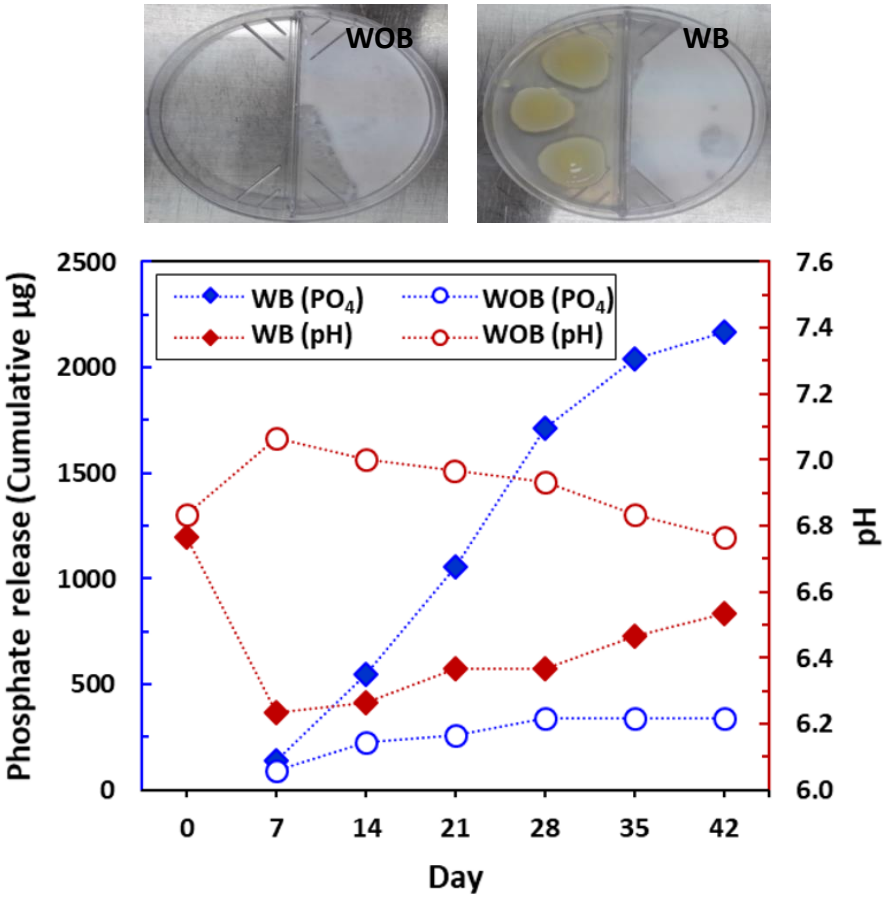

Figure 2. Effect of *Bacillus megaterium* VOCs on (A) pH and (B) phosphate release of HANP-containing suspension with incubation times. Abbreviation: WOB, without bacteria; WB, with bacteria. Means and standard deviations (n = 3) are shown.

Because the band of interest related to $\nu_{asym}(COO^-)$ overlapped with the bending mode of water, the HANPs were subjected to H/D exchange so that the surface-accessible OH species on the HANPs were replaced with OD, whose vibrations can be downshifted in frequency (Sakhno et al, 2015). The spectra of the materials recorded after this exchange are presented in **Fig. 3B**. Here, the OH stretching mode of the adsorbed water was replaced by the OD stretching mode within the 2760–1900 cm^{-1} range, and the water bending mode shifted to 1200 cm^{-1}, thus leaving the antisymmetric stretching mode of the carboxylate species unaffected. In particular, the spectrum of the sample at the earliest time point (7B) exhibited the Gaussian-like shape of either the ν_{asym} or ν_{sym} modes of COO^-. Further, an increase in time (14B) resulted not only in an increase in the intensity of the corresponding bands but also in changes to the shape of ν_{asym}, which now consisted of a band centered at 1633 cm^{-1} with a shoulder at higher wavenumbers (ca. 1663 cm^{-1}). At the last time point (28B), the changes in the shape of ν_{asym} could not be specifically quantified because the signal was out of scale. Interestingly, doubling the time of exposure of the HANPs to the MVOCs from one to two

weeks did not result in a noticeable increase in the intensity of the ν_{sym} signal, but rather led to the formation of a doublet. A possible explanation for this is that almost full surface coverage was reached after 14 days, with further exposure resulting in the reorganization of the carboxylate species on the surface, as evidenced by the appearance of the additional signal at 1330 cm^{-1}. Given the high sensitivity of these vibrations to the nature of the side groups of the acids and the types of acid–surface complexes (Arena et al., 2015), this is a strong indication of the presence of oxalic acid on the surface of the MVOC-treated samples.

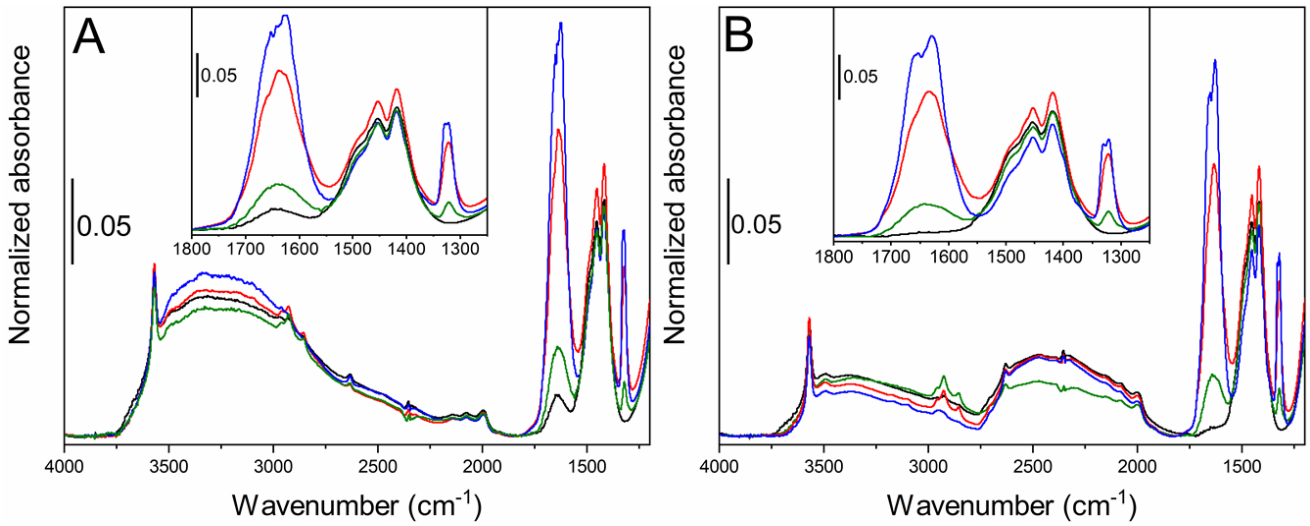

Figure 3. FT-IR spectra of the WOB (black curve, without bacteria), 7B (green curve, with bacteria for 7 days), 14B (red curve, with bacteria for 14 days) and 28B (blue curve, with bacteria for 28 days) samples, (A) after outgassing at beam temperature for 3 hours and (B) after D_2O exchange and subsequent outgassing at beam temperature for 3 hours.

In order to more clearly understand if the observed signals were comparable with those of oxalate species on the surface of MVOC-treated HANPs, a model experiment was carried out. HANPs were exposed to pure oxalic acid vapor and their IR spectrum was compared to the 14B sample (**Fig. 4**). Interestingly, there was good correspondence between the bands due to the antisymmetric and symmetric stretching of COO^- in the two spectra.

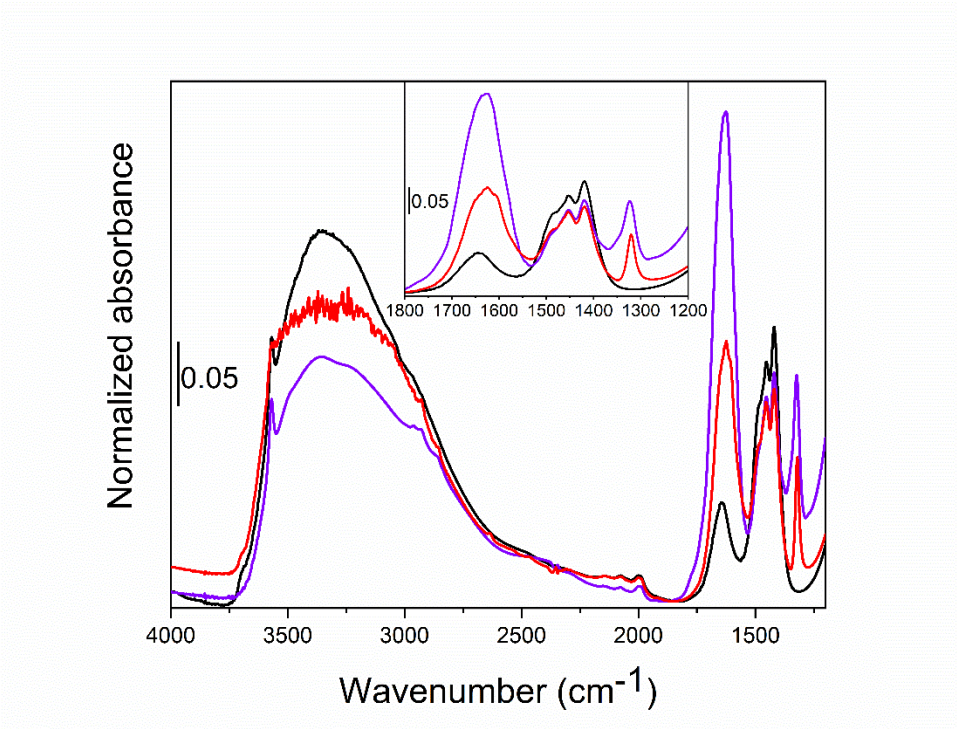

Figure 4. FT-IR spectra of the WOB (black curve, without bacteria), 14B (red curve, with bacteria for 14 days) and WOB with adsorbed oxalic acid (violet curve) samples. The spectra were acquired after outgassing at beam temperature for 2 hours

We then analyzed the crystal structure of the HANPs treated with MVOCs to determine whether it was modified by the adsorbed oxalic acid. The XRD patterns collected for each sample are presented in **Fig. 5**. The spectra revealed that all of the samples consisted of poorly crystalline HA as the main phase, with a crystallinity index calculated according to Equation (1) of 13.0%. Peaks typical of HA diffraction patterns (PDF card file 00-009-0432) were observed at a 2θ of 25.9°, 31.7°, 32.9°, 34.0°, 39.8°, 46.7°, 49.5°, and 53.1° corresponding to the lattice planes with Miller indexes of (0 0 2), (2 1 1), (3 0 0), (2 0 2), (3 1 0), (2 2 2), (2 1 3), and (0 0 4), respectively. All of the samples had a similar domain size along the (002) and (310) directions (38 ± 4 and 13 ± 2 nm, respectively). These results indicate that, similar to other examples of HA synthesized using wet precipitation reported in the literature (Adamiano et al., 2017; Stephanie et al., 2018; Marchiol et al., 2019), the crystallites are slightly elongated in the c-axis direction compared to the perpendicular a/b-axis.

The XRD patterns of the HANPs treated with MVOCs featured a small peak around 24.2°, indicating the presence of low levels of secondary phase (e.g., < 2.0 wt.%) that could not be quantified using Rietveld refinement (because the signal was too weak). The intensity of this peak, which was assigned to calcium oxalate (PDF card file 00-016-0379), in particular the lattice planes with a Miller index of (0 2 0), increased with the exposure time (*i.e.*, from 7B to 28B). This indicates that the longer the HANPs are exposed to MVOCs, the higher the quantity of calcium oxalate, although the levels of this secondary phase remain low.

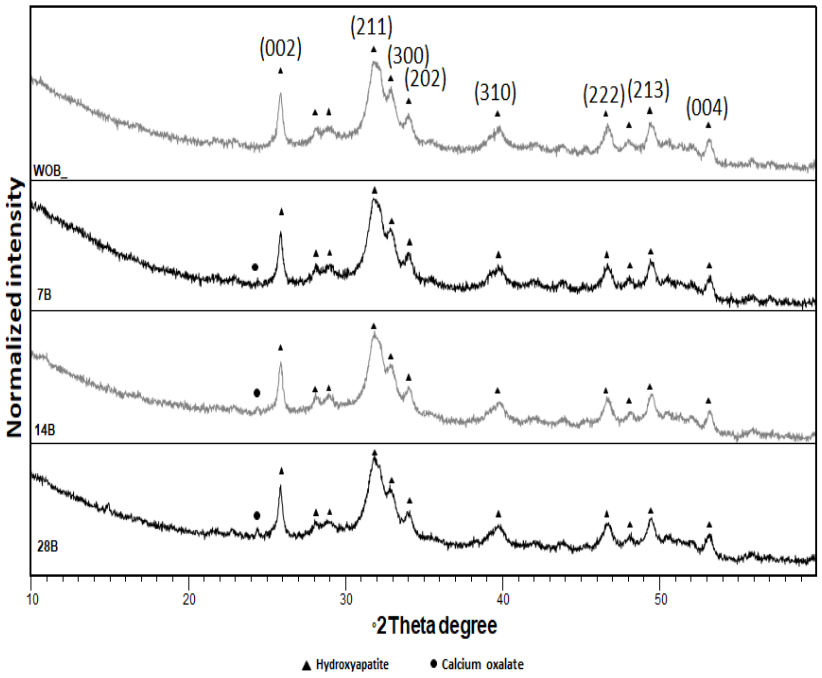

Figure 5. XRD pattern of the original HANPs (WOB, without bacteria) and that interacted with MVOCs (7B, with bacteria for 7 days; 14B, for 14 days; and 24B, for 24 days).

The results for the elemental analysis of the HANPs are summarized in **Table 1**. The HANPs had a similar composition before and after MVOC treatment, with the Ca/P ratio of all samples similar and slightly higher than that of stoichiometric HA (1.67). This lack of variation between the samples is primarily due to the low levels of calcium oxalate in the MVOC-treated HANPs; higher values are typical for partially carbonated HANPs in which the CO_3^{2-} anions present in the synthesis solution due to the dissolution of atmospheric CO_2 partially substitute PO_4^{3-} in the HA structures during the reaction between the calcium and phosphorous precursors.

Table 1. Chemical composition of WOB (without bacteria), 7B (with bacteria for 7 days), 14B (for 14 days), and 28B (for 28 days) determined by ICP-OES

	Ca		P			
Sample	**wt%**	**SD**	**wt%**	**SD**	**Ca/P**	**SD**
WOB	35.4	1.7	16.2	0.7	0.01	1.69
7B	35.9	1.2	16.4	0.5	0.01	1.70
14B	35.1	1.6	15.9	0.7	0.01	1.70
28B	36.2	0.1	16.1	0.1	0.01	1.73

SEM micrographs of the WOB and 28B samples are displayed in **Fig. 6A and 6B**, respectively. For the MVOC-treated samples, we only present representative images for the 28B sample because all of the samples were found to have similar features. The WOB sample exhibited the morphology and size typical of nanocrystalline HA, with needle-like particles with a length of 75−125 nm and a width of 15−25 nm. The HANPs treated with MVOCs had a similar structure but with the occasional occurrence of a small number of larger particles (circled in yellow in **Fig. 6B)**.

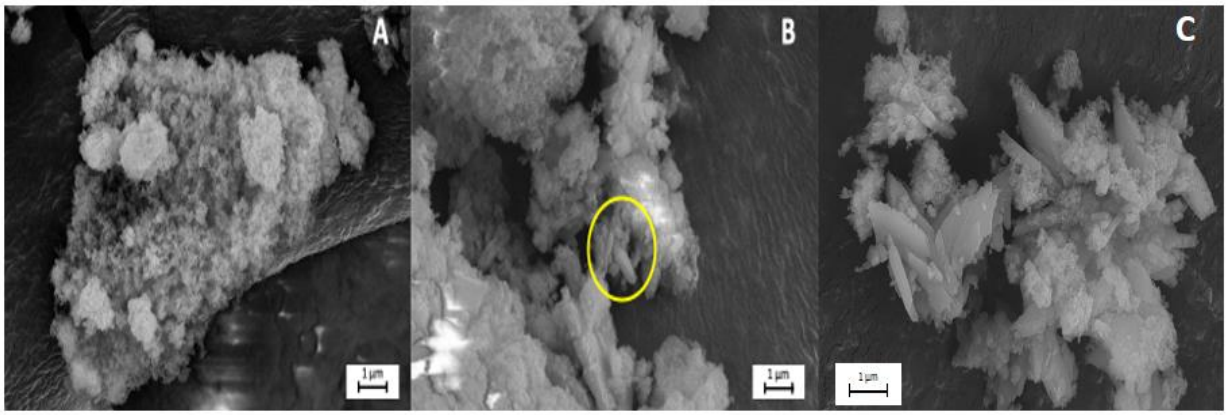

Figure 6. SEM pictures at 25,000 x magnification of samples (A) WOB (without bacteria) and (B) 28B (with bacteria for 28 days), and (C) 35,000 x magnification of samples 28B collected on platy crystals. The circle in yellow highlights the presence of calcium oxalate crystals

A micrograph of particles from the 28B sample at a higher magnification is presented in **Fig. 6C**. The crystals were characterized by a platy morphology with a prominent facet that was around 1.0 µm in width and length, with a thickness of around 0.15–0.25 µm. As reported in the literature, this morphology is typical of hydrated calcium oxalate crystals, also known as whewellite (Tazzoli et al., 1980). Thus, in accordance with the XRD data (**Fig. 5**), these particles were identified as hydrated calcium oxalate crystals.

These findings were confirmed by EDS analysis of the nanometric needle-like HA crystals of the WOB and 28B samples and the micrometric platy-like crystals of the 28B sample (**Table 2)**. The Ca/P ratio for the needle-like particles was close to that of stoichiometric HA for both samples. On the other hand, the Ca/P ratio for the platy crystals was significantly different from that for nanocrystalline HA, ranging between 1.50 and 1.75 for calcium deficient and carbonated HAs, respectively (Raynaud et al., 2002), while the C/Ca ratio was exactly the same as that for calcium oxalate. The formation of calcium oxalate in the presence of MVOCs would allow solubilized phosphate to be maintained because calcium ions are preferentially consumed to form calcium oxalate rather than calcium phosphates.

Table 2. EDS analysis of needle-like and platy crystals in (A) WOB (without bacteria) and (B) 28B (with bacteria for 28 days).

Sample	Ca/P	SD	C/Ca	SD
WOB	1.68	0.08	0.6	0.1
28B needle-like	1.65	0.05	0.8	0.2
28B platy-crystals	8	2	2.0	0.1

The greater phosphate release from HANPs treated with MVOCs inspired us to test whether the surface engineering of soil minerals associated with plant nutrition would lead to enhancement in plant growth. This question is important because previous reports demonstrating the positive effects of MVOCs on plant growth have regarded MVOCs as a molecular lexicon that is directly detected by plants. If other factors found in the soil environment mediate plant–microbe interactions, these previous results could be re-interpreted from a new mechanistic perspective.

The initial source of P in the MS agar was replaced with HANPs, and then the amount of available P was monitored as a function of incubation time with *B. megaterium*. As shown in **Fig. 7**, the pH fell and the levels of phosphate solubilized from the HANPs increased quantitatively. Given that the overall results were very similar to those obtained from HANPs in distilled water (**Fig. 2**), the release of P was not disrupted by the presence of other salts and plant nutrients. The percentage of HANPs that dissolved into phosphate ions by weight was found to be inversely proportional to the initial HANP levels, suggesting that an increase in the surface area of the HANPs in the MS agar was not directly proportional to the initial HANP levels.

A similar decrease in the pH was observed when *A. thaliana* was treated with MVOCs, while their combination led to significantly lower phosphate concentrations (**Fig. 8**). This indicates that plants in the presence of MVOCs can more efficiently absorb phosphate in gel systems; this was further substantiated by an increase in the fresh and dry weight of the plants (47% to 65% and 26% to 47%, respectively) in the presence of MVOCs (**Fig. 9**). The results also showed that both the fresh and dry weight of the plants significantly increased with an increase in the phosphate concentration from 2 to 6 mg. However, no significant change was observed at phosphate concentrations above 6 mg (**Fig. 9**), which may be due to saturation of the available P necessary for plant growth in a gel system. Overall, these results indicate that the higher release of P due to the MOVC-driven surface engineering of HANPs can improve plant nutrition and thus plant growth.

We then tested whether these results were reproducible in a real soil system. Soils mixed with three types of P-containing mineral (*i.e.*, HANPs**,** calcium phosphate dibasic, and micro-HA) were evaluated to determine whether the levels of available P are higher in the presence of MVOCs. During the testing, we maintained a constant concentration of total P in our soils systems (**Fig. S1**). Although the levels of available P in the calcium phosphate-treated soils were similar to those of the untreated soil on the first day, they increased significantly with longer incubation times (**Figs. 10 and S1**) both with and without MVOCs, though the phosphate release in the presence of MVOCs was significantly higher for all types of calcium phosphate. This indicates that MVOCs that are mobile and can diffuse into the soil matrix effectively modulate the P release kinetics of soil minerals. The concentration of the available P was also generally dependent on the quantity and size of the P-containing minerals, which suggests that the surface area of the minerals is critical to the P release kinetics. The sorption of MVOCs onto the mineral surfaces would activate the release of available P from the particles. The prolonged release effects with incubation times of up to 56 days were also typical of the surface engineering of P-containing ceramics (Samavini et al., 2018; Yoon et al., 2020; Yoon et al., 2021). It is important to note that the MVOC-induced increase in the available P in the soil occurred without adding calcium phosphate powder, indicating that the P-containing minerals within the soil are strongly affected by the MVOCs.

As shown in **Fig. 11**, the enhanced release of P increased plant growth, which was positively affected by the levels of P-containing minerals and the presence of MVOCs. The change in the phosphate concentration in soils with *A. thaliana* (**Fig. S2**) indicates that more phosphate was supplied to the plants via the MVOCs. In addition, the P content per unit mass of the plants was in accordance with the higher growth levels. Similarly, the concentration of the available P and total P in the soil was inversely proportional to the plant growth (**Fig. 12 and S3**). These data suggest that the MVOC-mediated increase in available P in the soil matrix is a direct influence on plant growth. Because plant nutrition is strongly associated with plant growth and stress resistance (Feller et al., 2018; Brumbarova et al., 2019), previous results demonstrating enhanced plant growth and stress resistance due to MVOCs should be re-evaluated to consider whether the soil minerals were modified. Experimental approaches to identify the molecular targets of MVOC-based plant stimulations should also be examined to determine whether plant nutrition is affected by soil mineral surface modification because plant nutrition coincides with changes in gene and protein expression (Brumbarova et al., 2019).

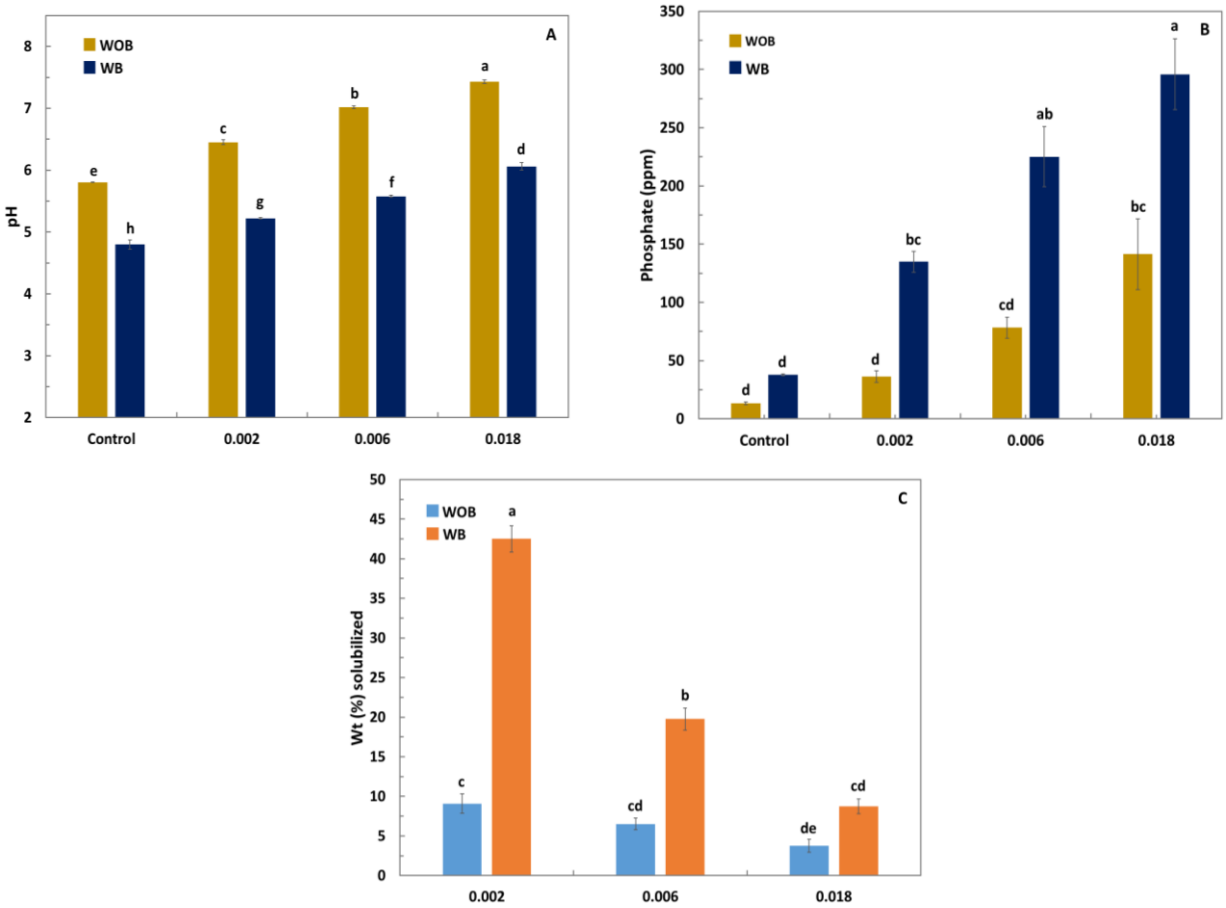

Figure 7. Variations of (A) pH and (B) phosphate concentration in the MS agar (15 mL) containing 0, 2, 6 and 18 mg of HANPs with *Bacillus megaterium* VOCs for 2 weeks. The agars were maintained without plants during the cultivation. Abbreviation: WOB, without bacteria; WB, with bacteria. Means and standard deviations (n = 3) are shown. Statistical analyses are based on LSD ($p < 0.05$).

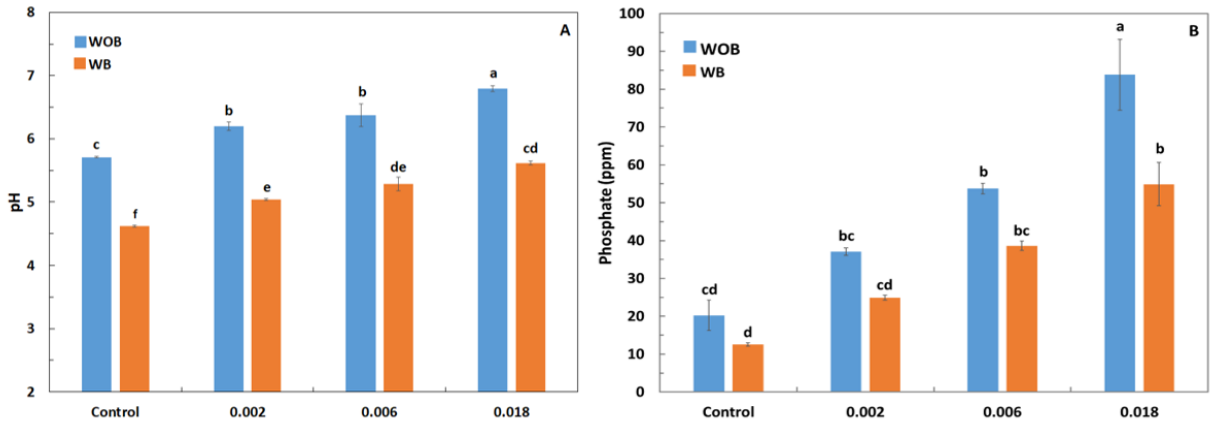

Figure 8. Variations of (A) pH and (B) phosphate concentration in the MS agars containing 0, 2, 6 and 18 mg of HANPs affected by VOCs of *Bacillus megaterium* and *Arabidopsis thaliana* seedlings for 2 weeks. Abbreviation: WOB, without bacteria; WB, with bacteria. Means and standard deviations (n = 3) are shown. Statistical analyses are based on LSD ($p < 0.05$).

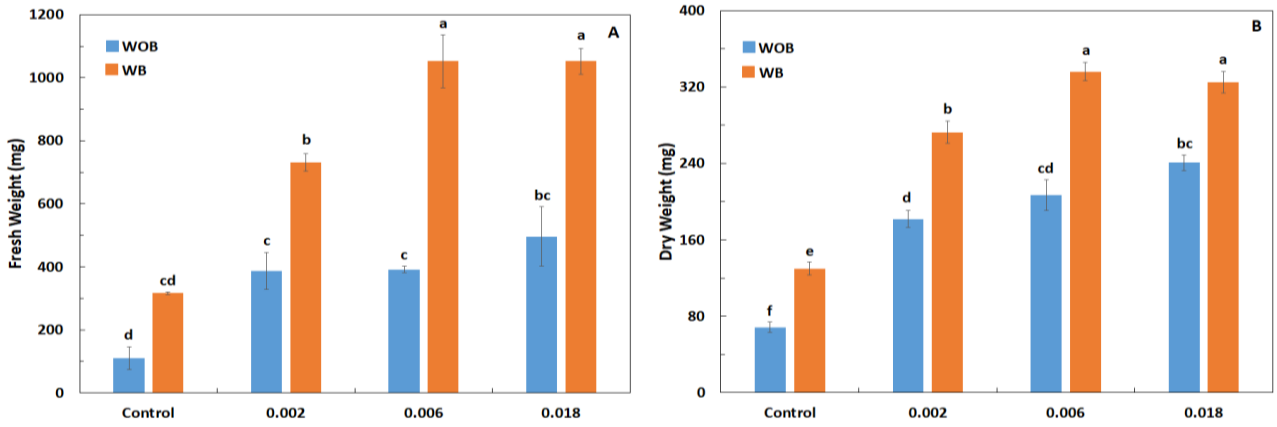

Figure 9. Effect of *Bacillus megaterium* VOCs on *Arabidopsis thaliana* growth (i.e., (A) fresh weights and (B) dry weight) on MS agars containing 0, 2, 6 and 18 mg of HANPs. Abbreviation: WOB, without bacteria; WB, with bacteria. Means and standard deviations (n = 3, each n contains 12 plants) are shown. Statistical analyses are based on LSD ($p < 0.05$).

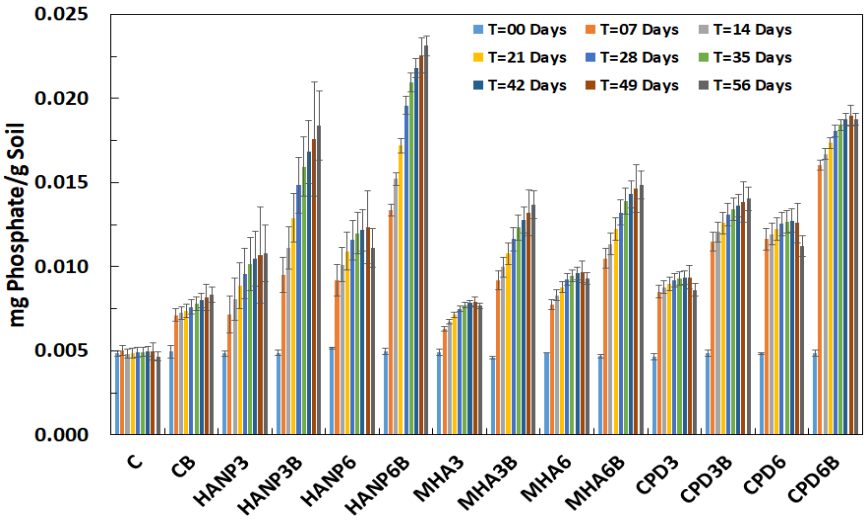

Figure 10. The effect of *Bacillus megaterium* VOCs on phosphate release from P-containing minerals (i.e., HANP, MHA, CPD) in soils for 56 days. Means and standard deviations (n = 3) are shown. Abbreviations: **C**: Bulk soil; **CB**: without P source + Bacteria; **HANP3B**: 3mg HANP + Bacteria; **HANP6B**: 6mg HANP + Bacteria; **CPD3B**: 3mg CPD + Bacteria; **CPD6B**; 6mg CPD + Bacteria; **MHA3B**: 3mg MHA + bacteria; **MHA6B**: 6mg + Bacteria; **HANP**: hydroxyapatite nanoparticle; **CPD**: calcium phosphate dibasic; **MHA**: micro hydroxyapatite

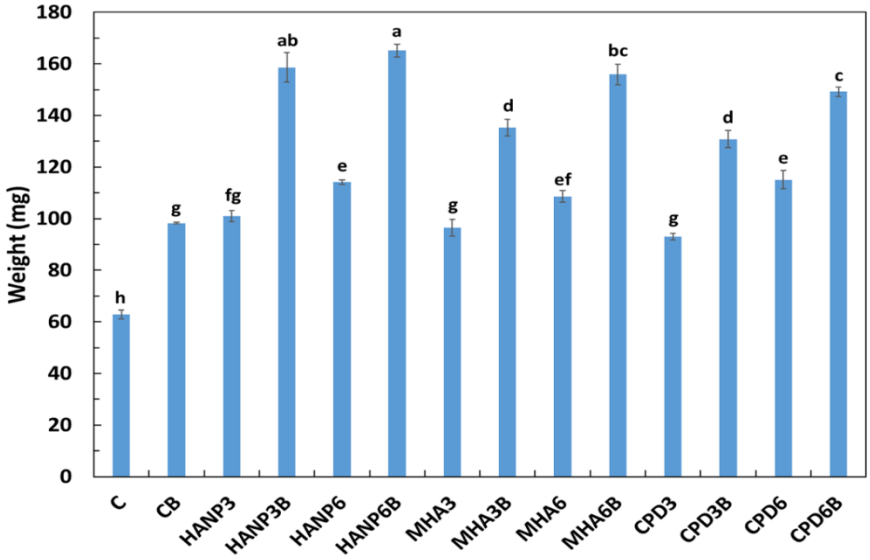

Figure 11. Biomass (dry weight) of *Arabidopsis thaliana* treated with HANP, MHA, and CPD in the presence and absence of *Bacillus megaterium* VOCs for 56 days. Means and standard deviations (n = 3, each n contains 6 plants) are shown. Statistical analyses are based on LSD ($p < 0.05$).

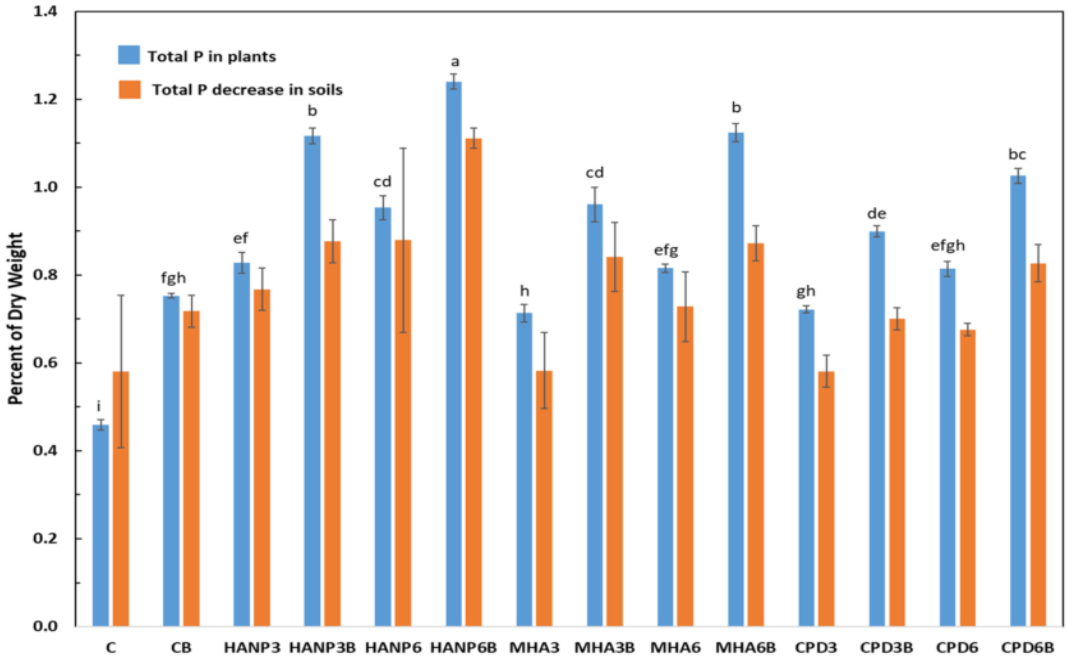

Figure 12. P contents of *Arabidopsis thaliana* and corresponding P decrease in soils treated with HANP, MHA, and CPD in the presence and absence of *Bacillus megaterium* VOCs for 56 days. Means and standard deviations (n = 3, each n contains 6 plants) are shown. Statistical analyses are based on LSD ($p < 0.05$).

Conclusion

This research demonstrated the direct interaction between MOVCs and P-containing ceramics, which can then affect plant nutrition. It is evident that specific types of MOVC containing oxygen-based functional groups are capable of modifying the surface of P-containing minerals including HANPs**,** calcium phosphate dibasic, and micro-HA, thus accelerating the release of soluble phosphate. By monitoring changes in pH and IR peak variations corresponding to COO^-, it can be concluded that this release is due to the combined actions of a lower pH and surface engineering by carboxylic group-containing MVOCs. These actions cause the minerals to become more soluble for a longer period of time. XRD and SED-EDS analysis also revealed the formation of calcium oxalate during the solubilization process, suggesting that oxalate is solidified when calcium ions are released. As a result, phosphate is maintained within the soil by inhibiting its recrystallization into calcium phosphates. The higher concentration of phosphate for longer periods was also observed in soil and gel environments, and the growth of *A. thaliana* was also promoted. Given that the modulation of plant nutrition affects many components of plant physiology, including versatile gene expression, our findings raise the need to confirm whether the previously reported effects of MVOCs on plants are due to changes in soil minerals associated with plant nutrition.

Acknowledgments

This work was supported by "BioGreen21 Agri-Tech Innovation Program (Project No. PJ01624001)" Rural Development Administration, Republic of Korea, and Korea Environment Industry & Technology Institute (KEITI) through project to develop eco-friendly new materials and processing technology derived from wildlife, funded by Korea Ministry of Environment (MOE) (2021003270006).

Conflict of interest

There is no conflict of interest.

References

Achelhi, k., Masse, S., Laurent, G., Saoiabi, A., Laghzizil, A., Coradin, T., 2010. Role of carboxylate chelating agents on the chemical, structural and textural properties of hydroxyapatite. Dalton Trans. 39(44), 10644-51. https://doi.org/10.1039/C0DT00251H

Adamiano, A., Fabbri, D., Falini, G., Belcastro, M.G., 2013. A complementary approach using analytical pyrolysis to evaluate collagen degradation and mineral fossilisation in archaeological bones: The case study of Vicenne-Campochiaro necropolis (Italy). J. Anal. Appl. Pyrolysis. 100, 173-180. https://doi.org/10.1016/j.jaap.2012.12.014

Adamiano, A., Sangiorgi, N., Sprio, S., Ruffini, A., Sandri, M., Sanson, A., Gras, P., Grossin, D., Frances, C., Chatzipanagis, K., Bilton, M., Marzec, B., Varesano, A., Meldrum, F., Kroger, R., Tampieri, A., 2017. Biomineralization of a titanium-modified hydroxyapatite semiconductor on conductive wool fibers. J. Mater. Chem. B. 5(36), 7608-7621. https://doi.org/10.1039/C7TB00211D

Arena, F., Deiana, C., Lombardo, F., Ivanchenko, P., Sakhno, Y., Trunfioa, G., Marta, G., 2015. Activity Patterns of Metal Oxide Catalysts in the Synthesis of N-Phenylpropionamide from Propanoic Acid and Aniline. Catal. Sci. Technol. 5(3), 1911-1918. https://doi.org/10.1039/C4CY01504E

Brumbarova, T., Ivanov, R., 2019. The nutrient response transcriptional regulome of arabidopsis. iScience. 19, 358-368. https://doi.org/10.1016/j.isci.2019.07.045

Chang, S. C., Jackson, M. L., 1957. Fractionation of soil phosphorus. Soil Sci. 84, 133-144

Choi, H.K., Song, G.C., Yi, H.S., Ryu, C.M., 2014. Field evaluation of the bacterial volatile derivative 3-pentanol in priming for induced resistance in pepper. J Che Ecol. 40(8), 882-92. https://doi.org/10.1007/s10886-014-0488-z

Diallo-Garcia, S., Osman, M.B., Krafft, J.M., Boujday, S., Guylene, C., 2014. Discrimination of infrared fingerprints of bulk and surface POH and OH of hydroxyapatites. Catal. Today. 226, 81-88. https://doi.org/10.1016/j.cattod.2013.11.041

Feller, U., Kopriva, S., Vassileva, V., 2018. Plant nutrient dynamics in stressful environments: needs interfere with burdens. Plant nutrient dynamics in stressful environment. 1-6.

Fincheira, P., Quiroz, A., 2018. Microbial volatiles as plant growth inducers. Microbiol. Res. 208. 63-75. https://doi.org/10.1016/j.micres.2018.01.002

Fleet, M.F., 2009. Infrared spectra of carbonate apatites: v2-Region bands. Biomaterials. 30(8), 1473-81. https://doi.org/10.1016/j.biomaterials.2008.12.007

Jamal, A., Khan, A., Sharif, M., Jamal, H., 2018. Application of different organic acids on phosphorus solubility from rock phosphate. JHPR. 2, 43-48. https://doi.org/10.18052/www.scipress.com/JHPR.2.43

Jones, S.E., Pham, C.A., Zambri, M.P., Mckillip, J., Carlson, E.E., Elliot, M.A., 2019. Streptomyces volatile compounds influence exploration and microbial community dynamics by altering Iron availability. mBio. 10(2), eoo171-19. https://doi.org/10.1128/mBio.00171-19

Kanchiswamy, C.N., Malnoy, M., Maffei, M.E., 2015. Chemical diversity of microbial volatiles and their potential for plant growth and productivity. Front. Plant Sci. 6, 151. https://doi.org/10.3389/fpls.2015.00151

Lee, B., Farag, M.A., Park, H.B., Kloepper, J.W., Lee, S.H, Ryu, C.M., 2012. Induced resistance by a long-chain bacterial volatile: elicitation of plant systemic defense by a C13 volatile produced by Paenibacillus polymyxa. PloS One. 7(11), e48744. https://doi.org/10.1371/journal.pone.0048744

Li, Y., Weng, W., 2008. Surface modification of hydroxyapatite by stearic acid: characterization and in vitro behaviors. J. Mater. Sci: Mater Med. 19(1), 19-25. https://doi.org/10.3390/plants10020238

Lin, T.F., Huang, H.I., Shen, FT., Young, C.C., 2006. The protons of gluconic acid are the major factor responsible for the dissolution of tricalcium phosphate by Burkholderia cepacia CC-A174. Bioresour. Technol. 97(7), 957-960. https://doi.org/10.1016/j.biortech.2005.02.017

Liu, X.M., Zhang, H., 2015. The effects of bacterial volatile emissions on plant abiotic stress tolerance. Front Plant Sci. 6, 774. https://doi.org/10.3389/fpls.2015.00774

Marchiol, L., Filippi, A., Adamiano, A., Esposti, L.D., Iafisco, M., Mattiello, A., Petrussa, E., Braidot, E., 2019. Influence of hydroxyapatite nanoparticles on germination and plant metabolism of tomato (Solanum lycopersicum L.): Preliminary evidence. Agronomy. 9(161), 161. https://doi.org/10.3390/agronomy9040161

Mino, L., Negri, C., Santalucia, R., Cerrato, G., Spoto, G., Martra, G., 2020. Morphology, Surface Structure and Water Adsorption Properties of TiO2 Nanoparticles: A Comparison of Different Commercial Samples. Molecules. 25, 4605. https://doi.org/10.3390/molecules25204605

Mino, L., Negri, C., Zecchina, A., Spoto, G., 2016. Photodegradation of Organic Pollutants on TiO2 P25 Surfaces Investigated by Transmission FTIR Spectroscopy Under In Situ UV-Vis Irradiation. Z. Phys. Chem. 30, 1441-1451. https://doi.org/10.1515/zpch-2015-0733

Nuri, O.M., Irannajad, M., Mehdilo, A., 2019. Effect of surface dissolution by oxalic acid on floatation behavior of minerals. J. Mater. Res. Technol. 8(2), 2336-2346. https://doi.org/10.1016/j.jmrt.2019.03.013

Raynaud, S., Champion, E., Bernache-Assollant, D., Thomas, P., 2002. Calcium phosphate apatites with variable Ca/P atomic ratio I. Synthesis, characterisation and thermal stability of powders. Biomaterials. 23(4), 1065-1072. https://doi.org/10.1016/S0142-9612(01)00218-6

Rodriguez, H., Gonzalez, T., Goire, I., Bashan, Y., 2004. Gluconic acid production and phosphate solubilization by the plant growth-promoting bacterium Azospirillum spp. Naturwissenschaften. 91(11), 552-555. https://doi.org/10.1007/s00114-004-0566-0

Sakhno, Y., Ivanchenko, P., Iafisco, M., Tampieri, A., Martra, G., 2015. A Step toward Control of the Surface Structure of Biomimetic Hydroxyapatite Nanoparticles: Effect of Carboxylates on the {010} P-Rich/Ca-Rich Facets Ratio. J. Phys. Chem. C. 119(11), 5928-5937. https://doi.org/10.1021/jp510492m

Samavini, R., Sandaruwan, C., De Silva, M., Priyadarshana, G., Kottegoda, N., Karunaratne, V., 2018. Effect of citric acid surface modification on solubility of hydroxyapatite nanoparticles. J. Agric. Food Chem. 66(13), 3330-3337. https://doi.org/10.1021/acs.jafc.7b05544

Sarda, S., Iafisco, M., Pascaud-Mathieu, P., Adamino, A., Montesi, M., Panseri, S., Marsan, O., Thouron, C., Dupret-Boris, A., Tampieri, A., Drouet, C., 2018. Interaction of Folic Acid with Nanocrystalline Apatites and Extension to Methotrexate (Antifolate) in View of Anticancer Applications. Langmuir. 34 (40) ,12036-12048. https://doi.org/10.1021/acs.langmuir.8b02602

Schulz, S., Schlawis C., Koteska, D., Harig, T., Biwer, P., 2020. Structural Diversity of Bacterial Volatiles. Bacterial Volatile Compounds as Mediators of Airborne Interactions. 93-121.

Schutze, E., Stella, G., Freese, D., 2020. Kinetics of Phosphorus Release from Vivianite, Hydroxyapatite, and Bone Char Influenced by Organic and Inorganic Compounds. Soil Syst. 4(1), 1-20. https://doi.org/10.3390/soilsystems4010015

Sharifi, R., Ryu, C.M., 2018. Revisiting bacterial volatile-mediated plant growth promotion: lessons from the past and objectives for the future. Ann. Bot. 122(3), 349-358. https://doi.org/10.1093/aob/mcy108

Stella, M., Halimi, M., 2015. Gluconic acid production by bacteria to liberate phosphorus from insoluble phosphate complexes. J. Trop. Agric. and Fd. Sc. 43, 41-53.

Tazzoli, V., Domeneghetti, C. 1980. The crystal structures of whewellite and weddellite: re-examination and comparison. Am Min. 65(3-4), 327-334.

Trombetta, D., Castelli, F., Sarpietro M.G., Venuti, V., Cristani, M., Daniele, C., Saija, A., Mazzanti, G., Bisignano, G., 2005. Mechanisms of Antibacterial Action of Three Monoterpenes. Microb Agents Chemother. 49(6), 2474-8. doi: 10.1128/AAC.49.6.2474-2478.2005

Wang, D., Xie, Y., Jaisi, D., Jin, Y., 2016. Effect of low molecular weight organic acids on the dissolution of hydroxyapatite nanoparticles. Environ. Sci Nano. 3(4), 768-779. https://doi.org/10.1039/C6EN00085A

Weisskopf, L., Schulz, S., Garbeva P., 2021. Microbial volatile organic compounds in intra-kingdom and inter-kingdom interactions. Nat. Rev. Microbial. 19(6), 1-14. https://doi.org/10.1038/s41579-020-00508-1

Wuenscher, R., Unterfrauner, H., Peticzka, R., Zehetner, F., 2015. A comparison of 14 soil phosphorus extraction methods applied to 50 agricultural soils from Central Europe. Plant Soil Environ. 61(2), 86-96. https://doi.org/10.17221/932/2014-PSE

Yoon, H.Y., Lee, J.G., Esposti, L.D., Iafisco, M., Kim, P.J, Shin, S.G, Jeon, J.R., Adamiano, A., 2020. Synergistic Release of Crop Nutrients and Stimulants from Hydroxyapatite Nanoparticles Functionalized with Humic Substances: Toward a Multifunctional Nanofertilizer. ACS Omega. 5(12), 6598-6610. https://doi.org/10.1021/acsomega.9b04354

Yoon, H.Y., Phong, N.T., Joe, E.N., Kwon, S., Son, E.J., Jang, K.S., Jeon, J.R., 2021. Crop root exudate composition-dependent disassembly of lignin-Fe-hydroxyapatite supramolecular structures: a better rhizosphere sensing platform for smart fertilizer development. Adv. Sustain. Sys. 2100113.

https://doi.org/10.1002/adsu.202100113

Zhao, G., Sheng, Y., Wang, J., Li, Z., Yang, J., 2018. Optimized digestion methods: organic phosphorus sequential extraction, total phosphorus, and nitrogen simultaneous determination in sediments. J. Soils Sediments. 18(5), 2072-2080. https://doi.org/10.1007/s11368-018-1959-6